

1 **Joint sensing of bedload flux and water depth by**
2 **non-invasive seismic data inversion**

3 **M. Dietze¹, S. Lagarde², E. Halfi³, J.B. Laronne³, J. M. Turowski¹**

4 ¹GFZ German Research Centre for Geosciences, Section 4.6 Geomorphology, Potsdam, Germany

5 ²Département de Géosciences, École Normale Supérieure, PSL Research University, Paris, France

6 ³Ben-Gurion University of The Negev, Department of Geography and Environmental Development, Unit
7 of Environmental Engineering, Beer Sheba, Israel

8 **Key Points:**

- 9 • We introduce a generic approach to inverting seismic records for flood water depth
10 and bedload flux
11 • Model deviations are 0.01–0.04 m (water depth) and 0.00–0.04 kg/sm (bedload)
12 throughout a range of synthetic data sets
13 • Our approach allows continuous, high resolution and near real time processing with
14 < 0.10 m (water depth) and < 0.02 kg/sm (bedload flux) deviation

Abstract

Rivers are the fluvial conveyor belts routing sediment across the landscape. While there are proper techniques for continuous estimates of the flux of suspended solids, constraining bedload flux is a much more challenging task, typically involving extensive and expensive measurement infrastructure or labour-intensive manual point measurements. Seismometers are potentially valuable alternatives to in-stream devices, delivering continuous high resolution data on the average behaviour of a given reach. In the last few years, two models were introduced to predict the seismic spectra generated by river turbulence and bedload flux. However, the models require estimating a large number of parameters and the spectra usually overlap significantly, which hinders straightforward inversion. Here we explicitly make use of the joint parameters of the two models and their partial overlap. We provide a set of functions as part of the R package 'eseis' that allow generic modelling of hydraulic and bedload transport dynamics from seismic data. The underlying Monte Carlo approach creates lookup tables of potential spectra, which are compared against the empirical spectra to identify the best fitting solutions. The method is validated against synthetic data sets and independently measured metrics from the Nahal Eshtemoa, Israel, a flash flood dominated ephemeral gravel bed upland river. Our approach reproduces the synthetic time series of water depth and bedload flux with average absolute deviations of 0.01–0.04 m (water depth) and 0.00–0.04 kg/sm (bedload flux). The example flash flood water depths and bedload flux are reproduced with respective average deviations of 0.10 m and 0.02 kg/sm. Our approach thus provides generic, testable, and reproducible routines for a quantitative description of key hydraulic and sediment transport metrics that are hard to collect by other techniques in a continuous and representative manner.

1 Introduction

Understanding the boundary conditions and non-linear dynamics of bedload transport by streams is essential for understanding process geomorphology and long term landscape evolution, but also from an engineering and hazard perspective, especially if the transport happens under episodic flood conditions. Accordingly, there has been significant effort in collecting instrumental data on important parameters determining flow characteristics and boundary conditions. Classic approaches involve either labour-intensive manual sampling (e.g., King et al., 2004; Bunte & Abt, 2005), or the permanent construction of monitoring infrastructure in the stream bed (e.g., Habersack et al., 2016). Any sensors within the stream need to be sufficiently resilient to maintain operation under the harsh conditions during flood events (Geay et al., 2017). Typical in-stream observatories include pressure gauges, temperature sensors and turbidity sensors. Bedload dynamics are monitored with time-resolving slot samplers (Cohen et al., 2010) and acoustic impact sensors, such as pipe microphones, geophones and accelerometers, or plate geophones (Mizuyama et al., 2010; Rickenmann, 2017). All acoustic bedload sensors, with the exception of hydrophones deployed in the water column (Geay et al., 2019), deliver direct and indirect data on the target parameters, provide point measurements or can at best be installed along a line crossing the channel (e.g., Hildale et al., 2014), whereas interest is often directed to the average dynamics of a given reach.

In recent years, a complementary approach has gained increasing attention: stream-side instrumentation with seismic sensors (Burtin et al., 2008; Barrière et al., 2015; Roth et al., 2016; Schmandt et al., 2017). Such sensors, typically off-the-shelf seismometers or geophones, are installed at a safe distance from the inundated channel and record the ground motion due to in-stream processes. A sensor can be deployed within less than an hour, record high resolution data continuously and autonomously for several months, and is, in principle, able to transmit the data in near real time to processing and evaluation facilities. Hence, seismic monitoring shows potential for recording bedload flux, which has recently been demonstrated under laboratory and fields conditions (Gimbert

et al., 2019; Schmandt et al., 2017). However, unlike signals derived from bedload impact sensors and similar to the soundscape of rivers recorded by in-stream hydrophones (Geay et al., 2017), seismic signals derive from a multitude of sources (e.g., Roth et al., 2017) and, therefore, the identification, extraction, and processing of signals to determine bedload flux is challenging.

Physical models have been suggested to predict the seismic frequency spectra due to bedload transport (Tsai et al., 2012) and due to hydraulic processes within a channel (Gimbert et al., 2014). Dietze (2018) has shown the principal method of using such physical models to infer water depth quasi continuously for creeks. This involved computing a lookup table of potential spectra that differ only due to changes in river depth and identification of the best reference data fits to the time series of empirical spectra. Here, we expand this approach to bedload flux, based on the notion that the spectra generated by turbulence and bedload transport should be sufficiently distinct (cf. Gimbert et al., 2014; Dietze et al., 2019). In our approach, fits of the empirical data with pre-calculated reference spectra are optimised based on random combinations of the target parameters. Applying the approach to a case study at the Nahal Eshtemoa, Israel, we show how seismic stations can be used to continuously estimate key hydraulic and bedload transport parameters. We explore the validity of the approach based on synthetic data and by comparing the model output against independent measurements of target parameters. We show the value of seismic stations to gather insight on the anatomy of bedload transporting floods, and discuss potentials and limitations of the technique.

2 Materials and methods

2.1 Study site and instrumentation

The Nahal (river) Eshtemoa is an ephemeral, flash flood dominated gravel bed river in the semi-arid northern Negev Desert, Israel, draining the southern Hebron mountains in a catchment of about 112 km². Close to the town of As-Samu, the stream crosses a gently undulating landscape in an alluvial valley. A straight, 5 m wide reach with 1 m high banks is instrumented by a comprehensive in-stream observatory (Laronne et al., 1992), including Reid-type slot samplers, plate geophones, a pipe microphone, water quality sensors and sampler, as well as pressure transducers for the determination of water depth and water surface slope. Since 2016, a Nanometrics TC120s broadband seismometer has been installed in the right bank (Fig. 1 a, b). It is sampled by a Nanometrics Centaur data logger at a recording frequency of 200 Hz and a gain of 2.

2.2 Computational environment

The R package 'eseis' (Dietze, 2018) is a free and open source toolbox for handling the work flow of generic environmental seismology. With the latest developer version (0.5.0) it contains models to predict the seismic spectrum due to turbulent channel flow (Gimbert et al., 2014), and impacting bedload particles (Tsai et al., 2012). Both models can be explored in an interactive graphical user interface (GUI) (Fig. 2). Three additional functions, denoted by the prefix *fmi*, are devoted to the approach of fluvial model inversion presented in this study. Data preparation, processing, analysis and visualisation steps were performed with R v. 3.5.3 (RCoreTeam, 2015). The R functions, data sets and utilised scripts are available as commented markdown files in the supplementary materials to reproduce the presented results.

2.3 Data processing

Flood water depth and bedload flux time series were recorded at minute resolution. The bedload flux time series starts when at least 4 kg of sediment have been collected in the slot samplers during an event, which represents the sensitivity threshold of the

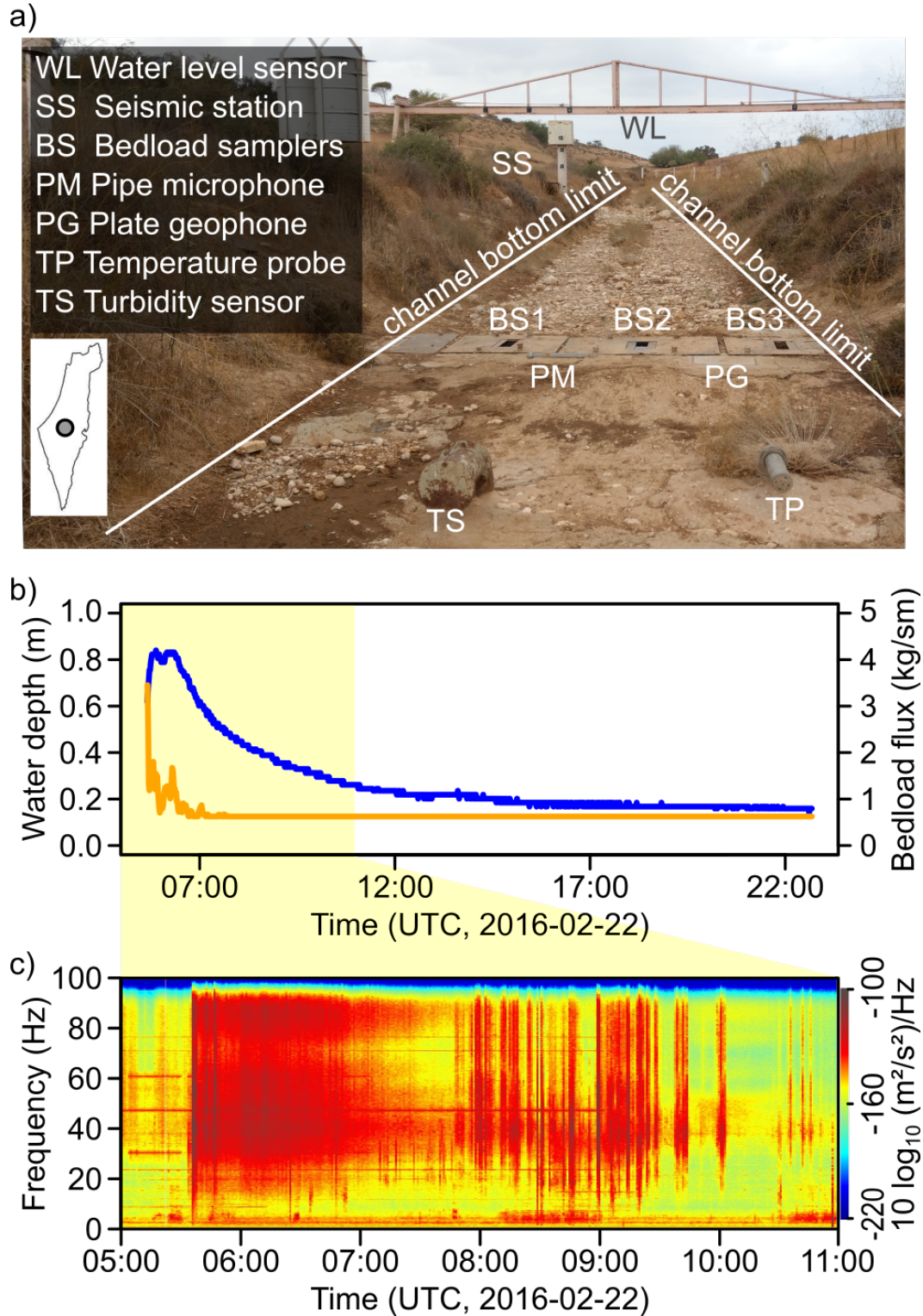


Figure 1. Study site, instrumentation and example flood event. a) View upstream of the flash flood prone Nahal Eshtemoa, Israel. At this location, an in-stream observatory records many essential hydraulic, sediment transport and chemical parameters. A broadband seismometer is installed at the true right bank. b) Hydrograph and bedload flux data from an example flood event; yellow background denotes period of interest. c) Spectrogram of the example flood as recorded by the seismometer.

115 sensors. We used the median of the values measured by the three bedload samplers to
 116 generate a representative bedload flux per unit stream width. The recorded seismic files
 117 were converted to hourly SAC files and organised in the consistent structure as used by
 118 the functions of the 'eseis' package. For the relevant part of the flood (05:40 to 11:00 UTC,
 119 cf. Fig. 1 b) we calculated a spectrogram from the vertical component of the seismic time
 120 series using the method of (Welch, 1967) with 10 s long, non-overlapping windows, av-
 121 eraging 5 s long and 80 % overlapping sub windows.

122 2.4 Model approach

123 Our approach assumes that the recorded seismic spectrum is dominated by chan-
 124 nel activity, i.e., a combination of turbulent flow and sedimentary particles impacting
 125 the channel floor during bedload transport, whereas other sources such as the effects of
 126 wind and rain, or anthropogenic activity are of subordinate importance. Under these con-
 127 ditions, we can exploit the combination of the seismic models of Tsai et al. (2012) and
 128 Gimbert et al. (2014). Specifically, we used a Monte Carlo approach to randomly vary
 129 the two parameters of interest, water depth and bedload flux, to generate 5000 differ-
 130 ent potential seismic conditions that serve as a look up table. In addition, to account
 131 for flow without bedload transport, we calculated another 1000 realisations where bed-
 132 load flux was set to zero and only water depth was varied. In the Nahal Eshtemoa case,
 133 we allowed water depth (h_w) to range from 0.01 m (minimum value required to allow
 134 model evaluation) to 1.20 m (120 % of bankfull depth). Bedload flux q_s was varied be-
 135 tween 0 kg/sm and 15 kg/sm (200 % of the range reported for other floods, (cf. Cohen
 136 et al., 2010)). The selected boundaries are arbitrary and can be extended, if needed –
 137 for example, when the model output yields values that clearly undershoot the expected
 138 empirical data. For each parameter combination, we calculated a seismic reference, and
 139 calculated root mean square errors with the corresponding observed spectrum. For each
 140 time step, we then selected the values for water depth and bedload flux corresponding
 141 to the artificial spectrum with the smallest root mean square error. To account for short
 142 term variability of the seismic record, the model results were smoothed with a running
 143 average (R package caTools v. 1.17.1.2, (Tuszynski, 2014)) using a window size of 18 sam-
 144 ples, i.e. 180 s.

145 2.5 Estimation of unknown model parameters

146 Both the turbulence (Gimbert et al., 2014) and the bedload (Tsai et al., 2012) model
 147 require constraints on a set of 17 parameters (Table 1). Some of these parameters can
 148 be determined from field measurements, namely the median grain size D_{50} (d_s), logarith-
 149 mic grain size standard deviation (s_s), channel width (w_w), channel bed gradient (a_w),
 150 and the distance between the centre line of the river and the seismic station (r_0). Other
 151 parameters can be estimated at reasonable accuracy based on prior measurements, such
 152 as the specific density of the fluid (r_w) and of the bedload material (r_s). And yet oth-
 153 ers are simply set according to computational needs and convention, such as the refer-
 154 ence frequency (f_0), frequency range (f) and resolution (res) for which the model yields
 155 results. Several parameters describe the seismic ground characteristics due to the site
 156 properties. This set of parameters (material quality factor q_0 and its increase with fre-
 157 quency e_0 , Rayleigh wave phase velocity at the reference frequency v_0 and its variation
 158 coefficient p_0 , and the Greens function displacement amplitude coefficients n_0) can be
 159 constrained by performing an active seismic survey. However, when that is not possible,
 160 they must be estimated.

161 In a first step we make use of the interactive GUI provided with the R package 'es-
 162 eis' (Fig. 2). This application allows changing all relevant model parameters and instan-
 163 taneously plots updated model outputs, together with an optionally provided empirical
 164 spectrum. We used this tool to explore the meaningful parameter space, which is able
 165 to create model spectra that match the overall shape and amplitude of a series of em-

Seismic spectra model visualisation

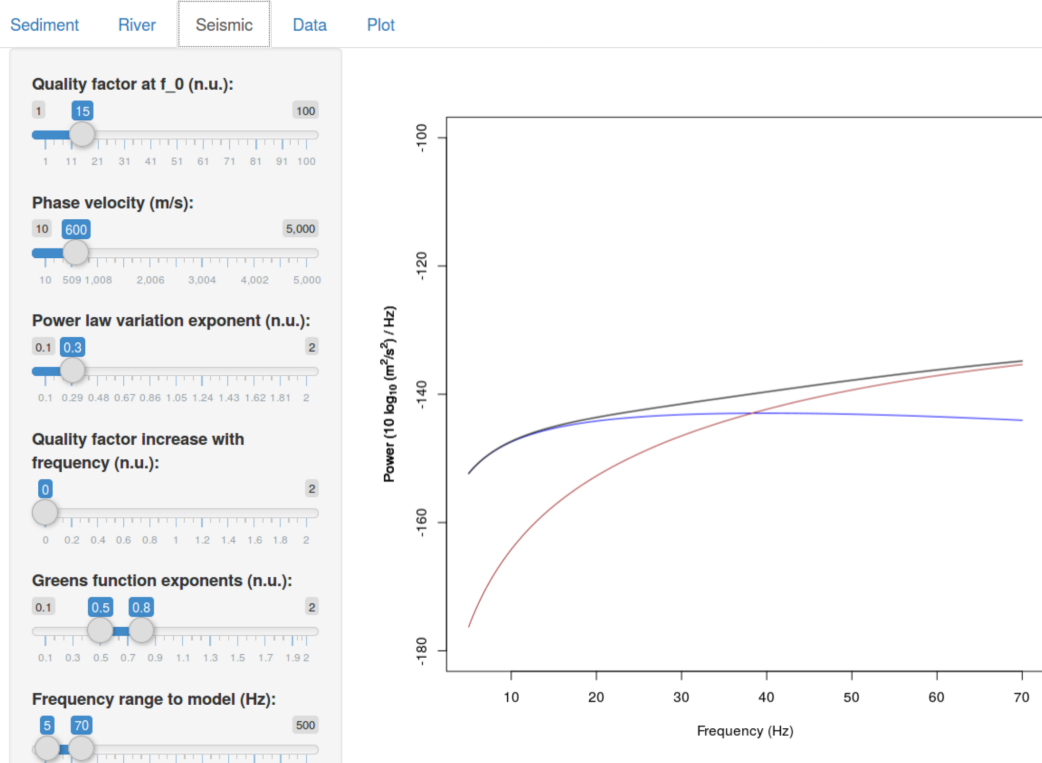


Figure 2. Interactive GUI of the seismic models, available through the R package 'eseis'. The application can be used to explore the effect of model parameters. It allows changing all relevant model parameters and generates instantaneous updates of the results. The blue line depicts the result of the water turbulence model, the red line shows the bedload model output and the black line illustrates the combined model spectrum.

Table 1. Model parameter values and their associated uncertainties. Target parameter ranges for identifying the most plausible ones are given in parentheses. * (Cohen et al., 2010)

Parameter (unit)	Symbol	Nahal Eshtemoa
D_{50} bedload grain diameter (m)	d_s	0.01*
Grain diameter standard deviation (log m)	s_s	1.35*
Bedload flux (kg/sm)	q_s	0–20
Sediment density (kg/m ³)	r_s	2650
Fluid density (kg/m ³)	r_w	1040
Water depth (m)	h_w	0.01–1.20
Average channel width (m)	w_w	5
Channel slope (radians)	a_w	0.0075*
Distance river to station (m)	r_0	5.5
Reference frequency (Hz)	f_0	1
Model frequency range (Hz)	f	10–70
Material quality factor at f_0 (s.d.)	q_0	16.77 (15–20)
Rayleigh wave phase velocity at f_0	v_0	859 (800–900)
Variation coefficient for v_0	p_0	0.62 (0.4–0.7)
Q increase with frequency (s.d.)	e_0	0.07 (0.01–0.25)
Greens function displacement amplitude coefficients (s.d.)	n_0	0.5, 0.8

166 pirical spectra. We focused on empirical spectra at the beginning of the flood event, where
167 sharp rises of broadband seismic signals (Tsai et al., 2012; Schmandt et al., 2017) indi-
168 cate pulses of bedload movement close the seismic sensor, and later stages of the flood,
169 when the bedload signal is no longer visible in the seismic spectrogram and most of the
170 seismic signal is presumably generated by turbulence. We adjusted the parameters q_0 ,
171 v_0 , p_0 , e_0 and n_0 to roughly match the shape of the resulting fluvial, bedload and joint
172 spectra to the empirical example spectra mentioned above. Thereafter, we changed the
173 parameters water depth and bedload flux to adjust the seismic power of the model spec-
174 tra until they visually matched the empirical spectra. The quality of the match was sub-
175 sequently quantified and optimised by minimising the root mean square error. From this
176 set of combinations optimized to first order we started changing the seismic parameters
177 towards lower and higher values, respectively, until the match of empirical and model
178 spectra obviously diverged. We defined these parameter ranges as the limits for the sub-
179 sequent step of parameter range optimisation. In a second step we performed the inver-
180 sion of the example flood data set in an extended Monte Carlo experiment. Since the
181 lower and upper Greens function parameters n_0 did not have significant impact on the
182 model spectra shape when changing them between 0.4 and 0.8 and 0.5 and 0.9, respec-
183 tively, we set them arbitrarily to 0.5 and 0.8. We created 10^5 random parameter com-
184 binations of the most sensitive parameters (q_0 , v_0 , p_0 , e_0) and the target parameters (h_w
185 and q_s), exploring the range of the former set of parameters to identify the most likely
186 values throughout the event (i.e., the medians of the distributions).

187 2.6 Model validation

188 In order to infer the ability of the model approach to estimate water depth and bed-
189 load flux, we created several synthetic data sets, inverted them and compared the result-
190 ing model time series of the target parameters to the input data (Fig. 3). Synthetic data
191 set 1 imposes a constant water depth of 0.5 m. The bedload is injected after 2 h of the
192 modelled time period (6 h), resulting in an instantaneous rise to 5 kg/sm, which is held
193 constant for another 2 h until it is reduced linearly to zero for the rest of the time. This
194 data set is mainly used to test the sensitivity of the model to fluctuations in a param-

195 eter when the other is changed. Synthetic data set 2 assumes synchronously rising and
 196 falling water depth and bedload flux, both of which are modelled as lognormal distri-
 197 bution curves. This scenario reflects a river where water depth and bedload flux do not
 198 show a hysteresis effect and where the seismic signal overlap is constant through time.
 199 Synthetic data set 3 features a lognormal bedload time series that rises steeper and nar-
 200 rower than the lognormal water depth time series, thus generating a bedload wave trav-
 201 elling in front of the flood wave. This scenario inherits a clockwise hysteresis pattern.
 202 Synthetic data set 4 uses the empirically measured water depth and bedload flux val-
 203 ues to generate a seismic spectrogram. It is used to explore how precisely the target vari-
 204 ables can be estimated by the model approach under ideal conditions: all signals of the
 205 spectrogram are only caused by flowing water and bedload flux.

206 Model quality is assessed by the absolute difference between synthetic and best fit
 207 modelled reference spectra. This error can be studied both in time and frequency space.
 208 Another measure of model quality is the error (residual) between water depth or bed-
 209 load flux and the respective model estimates.

210 **3 Results**

211 **3.1 Characteristics of the flood**

212 The flood hydrograph shows a rapid rise of water depth although the actual on-
 213 set of the event is not shown here because we define the event by the onset of the bed-
 214 load sampler records, i.e., at 05.40 UTC. After the flood’s double peak occurred (0.84
 215 and 0.83 m), water depth dropped logarithmically for at least 13 h (Fig. 1 b). The three
 216 bedload samplers monitored a maximum average value of 4.29 kg/sm. The highest bed-
 217 load fluxes were recorded within the first two minutes. Thereafter values declined pro-
 218 gressively to almost zero around 05:55 UTC, when two further, smaller bedload waves
 219 (peak flux 1.08 kg/sm) emerged for 30 min. Bedload transport ceased at 07:10 UTC. With
 220 the onset of the flood, the seismic spectrogram shows a broadband (10–90 Hz) increase
 221 in seismic power up to -100 dB, which progressively grades into background for about
 222 one hour. At about 07.50 UTC, a period of broadband spike appearance occurs that lasts
 223 for at least 2.5 h.

224 **3.2 Model validation with synthetic flood time series**

225 The ability of the model to reconstruct the synthetic time series of target param-
 226 eters (which were used to generate noise-free spectrograms that were inverted) provides
 227 the accuracy baseline for the actual inversion of the empirical data set. Synthetic data
 228 set 1 (Fig. 3 a) yielded absolute differences between best fit model and input spectro-
 229 gram of less than 0.5 dB and target parameter errors of 0.02 ± 0.04 m (water depth) and
 230 -0.03 ± 0.06 kg/sm (bedload flux). The modelled time series resemble the onset of changes
 231 and are only slightly affected by changes in the corresponding parameter. Synthetic data
 232 set 2 (Fig. 3 b) has only minor spectral differences (less than 0.26 dB) and model errors
 233 (0.02 ± 0.04 m and -0.06 ± 0.13 kg/sm, respectively). The concurrent changes in water depth
 234 and bedload flux are captured well. However, during the second half of the synthetic event
 235 the model produced increasingly larger deviations. Synthetic data set 3 (Fig. 3 c) has
 236 the largest spectral differences (up to 1.75 dB), but yielded the smallest target param-
 237 eter errors (-0.01 ± 0.03 m and -0.001 ± 0.03 kg/sm, respectively). These errors mainly ap-
 238 pear towards the end of the synthetic data set, when the continuously declining water
 239 depth curve is represented by step-wise model results. The synthetic data set produced
 240 by the real world time series of water depth and bedload flux (Fig. 1 b) produced spec-
 241 tral differences of up to 0.47 dB and target parameter errors for water depth and bed-
 242 load flux of -0.04 ± 0.03 m and -0.001 ± 0.02 kg/sm, respectively. The water depth is thus
 243 overestimated, especially when bedload transport ceases.

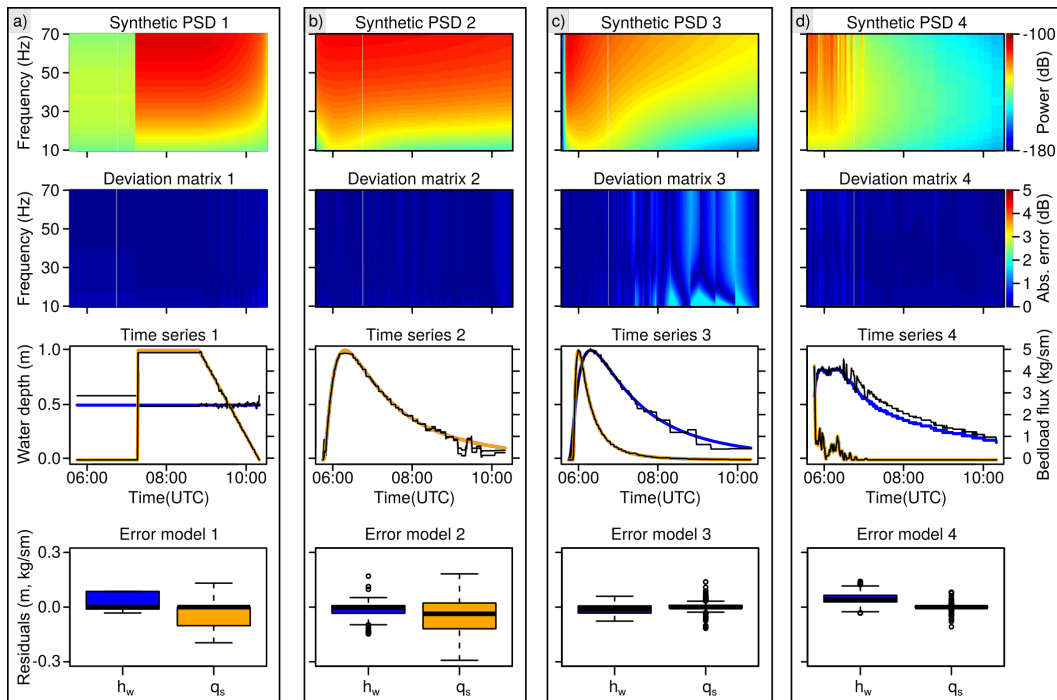


Figure 3. Model validation summary. Four synthetic data sets were tested, and are organised by columns a-d). Each panel shows the resulting synthetic spectrogram, the fit deviation matrix depicting the root mean square error between empiric spectra and best fit reference spectra, the input (blue line shows water depth, orange line bedload flux) and modelled time series (black lines), and the distribution of model errors (residuals) in target parameter units.

244

3.3 Model parameter estimation

245

246

247

248

249

250

251

252

253

254

255

256

257

258

259

260

261

Explorative model parameter adjustments (Fig. 2) revealed that the shape of the fluvial and bedload model spectra can vary significantly. In turn, the parameter range that lets the models and their summed effect converge in shape to those of the empirical spectra during the peak water depth and the falling limb of the flood is small. Thus, we defined the limits within which q_0 was allowed to vary to 15–20, for v_0 to 800–900 m/s, for p_0 to 0.4–0.7 and for e_0 to 0.01–0.25 (cf. Tab. 1). As expected, changes in the input parameters water depth and bedload flux result in amplitude shifts with no visible effects on the shape of the spectrum (Fig. 4 a). In contrast, higher ground quality factors (Fig. 4 b) lead to systematic counter-clockwise rotation effects of the spectra until the spectral power rises monotonously with increasing frequency, which is not visible in the empirical data (Fig. 1 c). A similar effect occurs for the Rayleigh wave phase velocity v_0 (Fig. 4 c), although increasing velocity values do not cause higher spectral power as is the case for the quality factor. The wave velocity variation coefficient p_0 (Fig. 4 d) mainly affects the amplitude of the bedload spectrum and the convexity of the turbulence spectrum. The parameter describing quality factor increase with frequency e_0 (Fig. 4 e) shows similar effects with value changes like the quality factor. However, this parameter is not included in the turbulence model and has therefore no effect on the latter.

262

263

264

265

266

267

268

269

270

Running the Monte Carlo approach with the range of seismic parameters as defined in Tab. 1 yielded convergent results with median values and quartiles of the distributions well within the defined parameter range (Fig. 4 f). The effect of the parameters is independent of each other. Thus, the best fitting combination of parameters for each of the 10 s long empirical spectra can in principle be anywhere within that imposed range. Since this is not the case the parameter distribution is assumed to be unimodal and adequately represented by the median as a most likely value. Therefore, we chose the medians ($q_0 = 16.77$, $v_0 = 859$, $p_0 = 0.62$, $e_0 = 0.07$) for the subsequent Monte Carlo run to estimate the actual target parameters.

271

3.4 Model results for the empirical data set

272

273

274

275

276

277

278

279

280

281

282

The seismic data of the example flood event (Fig. 1 c) shows contribution of the expected frequency bands between 5 and 70 Hz (Tsai et al., 2012; Gimbert et al., 2014; Schmandt et al., 2017). However, above 70 Hz there is increased seismic energy. That pattern appears to be a horizontally flipped version of the < 70 Hz signals and cannot be physically explained. Therefore, and to avoid introducing a systematic bias, we truncated the spectrogram to the frequency range 10–70 Hz, an interval to which the seismic models are most sensitive. Furthermore, to reduce scatter in the frequency domain and to improve computational speed (the frequency vector of the raw spectrogram had 1000 values), we spline-interpolated the frequency vectors of the spectrogram to 100 values between 5 and 70 Hz, corresponding to the modelled spectra (cf. supplementary materials I).

283

284

285

286

287

288

The best fit spectra deviations (Fig. 5 b) range between 0 and 15 dB. The highest deviations appear at the continuous narrow band signals (23, 47 Hz) as well as during the period with numerous short term, broadband signals (7:50–10:10 UTC). Smaller deviations, up to 10 dB occur during the early stage of the flood (5:40–7:50 UTC). They affect the upper and lower frequencies of the modelled spectra as well as the central bands (30–45 Hz).

289

290

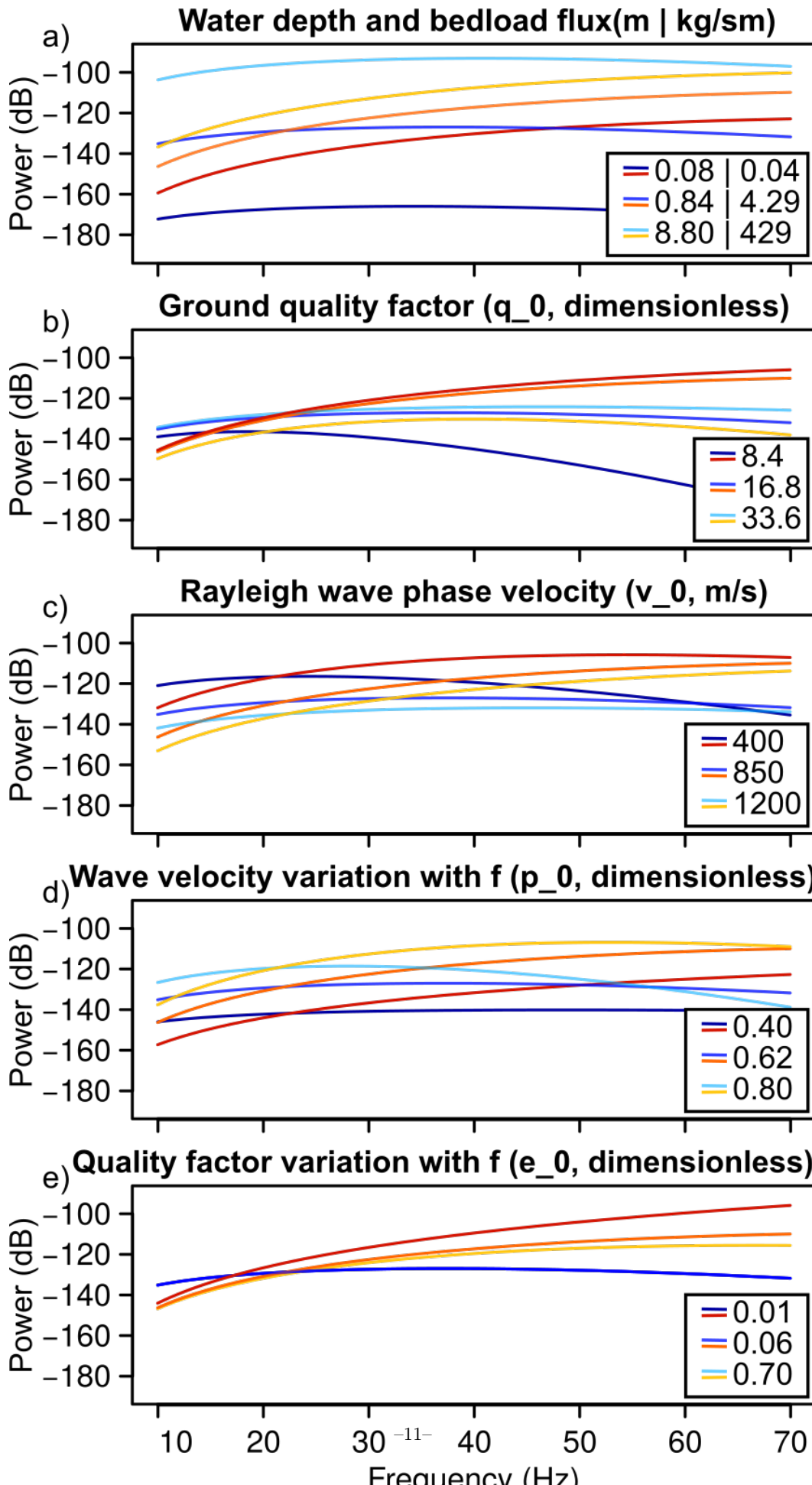
291

292

293

294

The modelled water depth (Fig. 5 c) is in general agreement with the independent water depth measurements, although the falling limb of the flood is underestimated by 0.10 m on average (i.e., median of the absolute deviations). During 7:50 and 10:10 UTC (grey polygon in Fig. 1), when the spectrogram (Fig. 5 a) exhibits several broadband spikes, the model shows significant overestimation effects. Overall, the seismic results are more variable than the one minute resolution control data (180 s running standard deviations



of 0.041 versus 0.029 m). Results of seismic bedload flux are also in the same range as the slot sampler data (0.02 kg/sm average deviation), and most of the short excursions of increasing and decreasing bedload flux values in the slot sampler time series are coincident with the seismic model results, both in terms of timing and amplitude.

4 Discussion

4.1 Model quality

The synthetic data sets (Fig. 3) allow insight on three different dimensions. First, they show the general applicability and validity of the Monte Carlo-based inversion approach. Second, they provide the baseline of accuracy, i.e., the minimum deviations to expect when modelling an empirical data set. Third, the scenarios allow insight as to how different combinations of flood and bedload flux evolutions appear in seismic spectrograms.

In all cases, the input time series were depicted by the model, with deviations of less than 0.04 m for water depth and 0.04 kg/sm for bedload flux. Thus, for inversions of empirical data sets one should anticipate at least these ranges of model deviations. Under the ideal conditions of synthetic data sets generated without any noise or contribution of additional seismic sources, the deviations of the best fit reference spectra from the synthetic spectra time series (deviation matrices in Fig. 3) are negligible. An exception is test data set 3 (Fig. 3 c), which shows misfits of up to 2 dB coincident with the step-like evolution of the modelled water depth during times of virtually zero bedload flux. This step-like behaviour disappears when more than the 1000 Monte Carlo cycles are used to generate the reference spectra (not shown). Thus, it is important to provide a sufficiently large number of potential parameter combinations for the reference spectra, especially when high fit qualities for the falling water depth limb are of interest. A similar effect is visible in the fourth synthetic data set (Fig. 3 d) and, to a lesser degree also in data set 2, where the falling water depth curve is systematically overestimated as soon as bedload flux fades.

The imposed time series of synthetic data set 1, constant water depth and a step-like onset of bedload movement, are far from what one would expect in natural systems. However, this scenario shows that model deviation is systematically higher for times when only one of the two expected seismic sources is active (i.e., water depth is overestimated when no bedload is transported). In the case of synchronous evolution of flood stage and bedload flux (data set 2) the model results maintain this synchronicity. This is encouraging because when a seismically derived data set exhibits such a pattern it is difficult to judge merely from the properties of the spectra, whether there indeed are two seismic sources present. In the case of a bedload wave travelling in front of a flood (Fig. 3 c), i.e., a clock-wise hysteresis pattern in the h_w-q_s relationship, the combined effect of turbulence and bedload movement result in a spectrogram with a trend of rising dominant frequency with time. Such patterns were observed in natural settings, such as a flash flood observatory in New Mexico (Dietze et al., 2019) but could not be attributed to a likely cause. Here, we can provide this cause, which is simply the combination of two seismic sources with different time evolution paths. The trend towards higher frequencies remains visible without any hysteresis effect, albeit weaker (e.g., Fig. 3 b). Since even water depths up to 0.5 m only contribute as much as -135 dB to the total seismic signal (Fig. 3 a), it appears that most of the seismic energy is contributed by the bedload part at this distance of channel to sensor.

4.2 Evolution of the flood event

The example event shows the typical features of flash floods in the Nahal Eshtemoa (Halfi et al., 2018): a suddenly rising water depth that remains unstable due to the

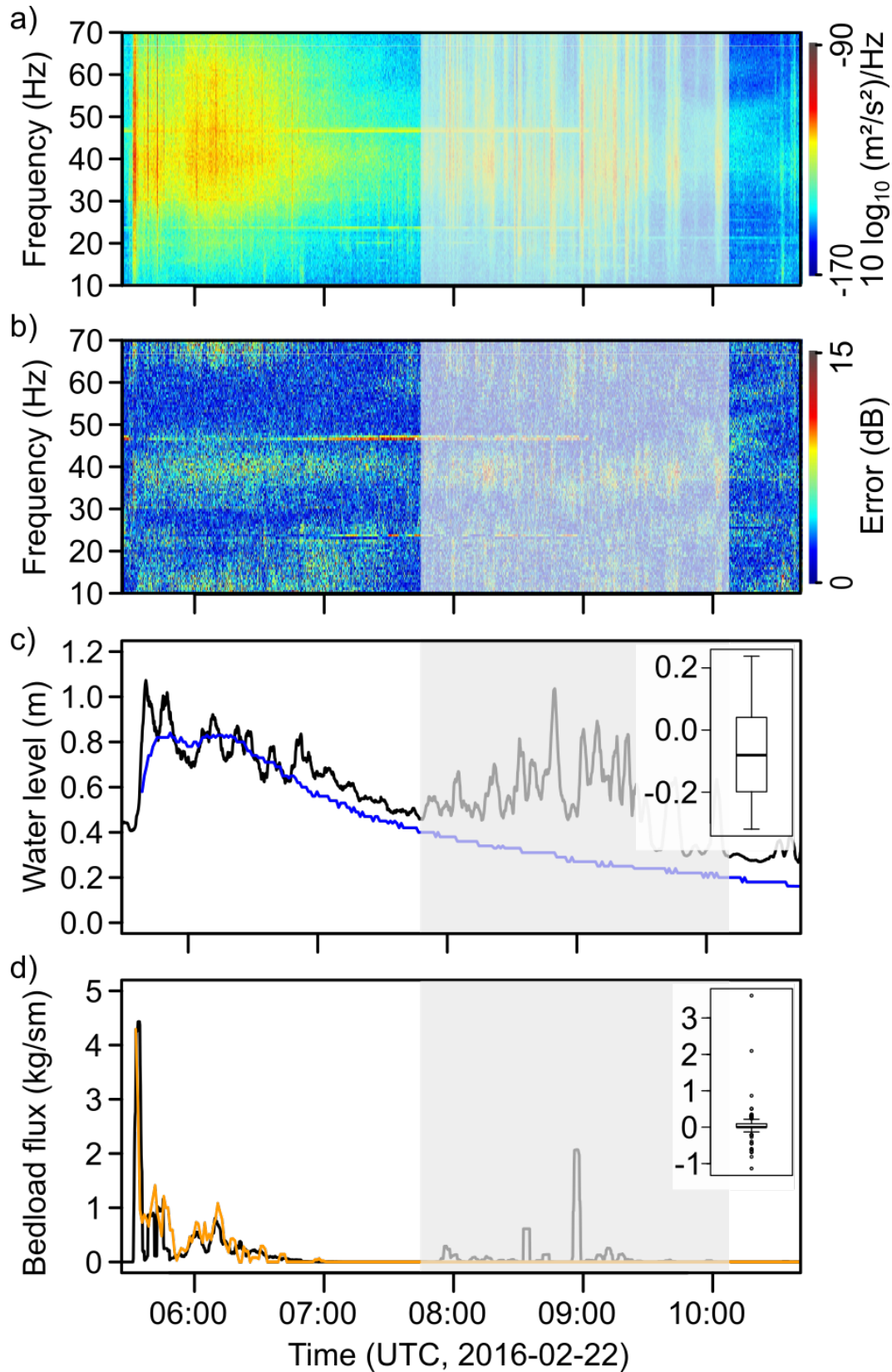


Figure 5. Results of the empirical data set inversion. a) Truncated (10–70 Hz) and aggregated (100 frequency values) spectrogram. b) Deviations of model fits resolved by time and frequency. c) Modelled (black line) and empirically measured water depth (blue line). d) Modelled (black line) and independently measured (orange line) bedload flux values. Note that in c) and d) the model results are smoothed by a 180 s running average filter. Grey polygons indicate a period with signal contamination. Boxplots give residuals of model versus empirical data.

344 high turbulence and a bedload bore at the front of the flood, occasionally followed by
 345 further bedload bores. The passing of these bores are recorded in the example flood by
 346 both the slot samplers and the seismic sensor (Fig. 5 d and a), the latter showing this
 347 as broadband spikes of seismic energy after the onset of the flood. With the end of the
 348 bedload transport period the spectrogram only shows noticeable seismic energy between
 349 20 and 50 Hz that gradually decreases in amplitude with time.

350 This trend is interrupted between 07:50 and 10:10 UTC (grey shaded area in (Fig. 5)
 351 by recurring broadband seismic pulses. We interpret these pulses as the effects of per-
 352 sons working at the observatory for data collection and station maintenance reasons. These
 353 activities included walking and operating at close proximity to the seismic sensor and
 354 a car idling at the bank. A further set of seismic signals, the temporally constant, nar-
 355 rowband horizontal lines in the spectrogram (Fig. 1 c) around 22 and 44, 30 and 60 Hz,
 356 is interpreted as the signature of measurement devices operating at the observatory. When
 357 excluding this period of signal contamination, the temporal variation of the seismic signal-
 358 derived bedload flux shows three important components of the average-channel bedload
 359 flux: (i) A first very large wave in bedload flux up to 5 kg/sm, which drastically recedes
 360 within minutes of the arrival of the flood bore, (ii) a second multiple-rise peaking at about
 361 1 kg/sm, and (iii) and a third, smaller rise (0.5 kg/sm) with a long, 1 h recession. Given
 362 the 120 s averaging required with respect to the sensitivity of the slot sampler bedload
 363 monitoring equipment, it is remarkable that a single sensor deployed on the bank of a
 364 river can determine the main and relative features of bedload flux.

365 4.3 Benefits, limitations and outlook

366 In comparison to classic approaches to constraining hydraulic and sediment trans-
 367 port parameters in fluvial systems the seismic method introduced here shows several ad-
 368 vantages. The sensors can be deployed easily and quickly, at a safe distance from the haz-
 369 ardous conditions of flood-prone streams. Modern seismic stations can record ground mo-
 370 tion data at high frequency, under harsh conditions and even transmit the data in near
 371 real time to analysis facilities where they can be automatically analysed. In the case shown
 372 here, and once the data set of reference spectra is pre-calculated, inverting an empiri-
 373 cal spectrum requires less than one second computation time on a single CPU. Thus, ef-
 374 ficient and near real time information about floods and the potentially hazardous bed-
 375 load they transport can be provided also for remote locations in a continuous manner.

376 While classic approaches, such as slot samplers are only able to measure the bed-
 377 load flux at discrete cross-sectional intervals (the slot aperture in the Nahal Eshtemoa
 378 observatory is 11 cm and the devices are spaced about 1 m) and a representative esti-
 379 mate of bedload flux must be based on averaging data of several samplers, the seismic
 380 approach implicitly provides an estimate for a longer reach. The size of that reach may
 381 be approximated by changing the parameter distance to river r_0 in the interactive GUI
 382 (Fig. 2). However, a more robust field experiment with actively moved pebbles in the
 383 channel would be more appropriate (cf. Schmandt et al., 2017).

384 None of the available bedload formulae can replicate such natural fluvial sediment
 385 wave phenomena as presented here (e.g., Gomez et al., 1989; Cudden & Hoey, 2003), even
 386 though theoreticians, notably Einstein (1950) and experimentalists (e.g., Iseya & Ikeda,
 387 n.d.; Lisle et al., 2001; Aberle et al., 2012; Ghilardi et al., 2014; Dhont & Ancey, 2018)
 388 have long been aware of their presence. Indeed, based on a century of geomorphologi-
 389 cal research, it is known that fluvial systems are complex (Schumm, 1991, 2005); they
 390 do not transport bedload at certain time scales as simply as does an "efficient" machine
 391 (Bagnold, 1966), nor merely determined by average reach shear stress (Parker, 1990).
 392 Instead, the fluvial system responds in complex manners, as in this case one sensor and
 393 the respective technique demonstrate. With the seismic approach we are able to provide
 394 robust and high resolution field data which are crucial to determine river activity, river

395 stability, river change and the transport of bedload to various ecologically sensitive reaches,
396 to reservoirs and to the oceans.

397 However, in comparison to classic methods, the seismic approach also has draw-
398 backs. First, the recorded signals represent measurements of ground velocity due to a
399 multitude of sources, which are inverted for the parameters of interest using a combi-
400 nation of physical models. These models are formulated under a series of assumptions
401 (cf. Tsai et al., 2012; Gimbert et al., 2014) and require information about a large num-
402 ber of parameters. Although the model output is in appropriate physical units (m and
403 kg/sm) that does not require development of a further transfer function, they are not
404 direct measurements of the parameters of interest. This point also needs to be consid-
405 ered in the light that the seismic approach does not necessarily reflect the same process
406 as, for example the Reid type sampler, which records all particles that fall through the
407 11 cm wide slot while omitting all particle that pass between two such slots. The seis-
408 mic record is an amalgam of the impacts of all bedload particles in a given reach and
409 therefore provides a spatially integrated result, which may differ from spatially discrete
410 direct measurements due to cross sectional non-uniform bedload fluxes.

411 The selection of seismic model parameters is crucial for the inversion results. Thus,
412 at best one performs an active seismic survey to independently constrain these param-
413 eters. Since this was not possible in this study, we introduced a step-wise approach as
414 an alternative: i) visual exploration of parameter effects on model output with respect
415 to empirical seismic observations under partly known flood conditions (Fig. 2), ii) long
416 Monte Carlo chains to identify the parameter combination that best explains the em-
417 pirical data set (Fig. 4 f), before iii) actually inverting the data with the most plausi-
418 ble set of parameters (Fig. 5) along with relevant metrics for model errors.

419 Seismic sensors are not only subject to the seismic sources of interest but also record
420 a range of further processes, as the period of maintenance activities shows. Atmospheric
421 processes such as wind and rain (Dietze et al., 2017; Roth et al., 2017) generate seismic
422 signals in a similar frequency range. Burtin et al. (2008) and Cook et al. (2018) showed
423 that the seismic footprint of rivers and the bedload they transport can be detected over
424 tens of kilometres. Thus, trunk streams close-by may also add their seismic signature
425 to the signals recorded at the stream of interest. Therefore, the deployment site for a
426 seismic station intended to record water depth and bedload flux must be chosen with care.
427 They should be out of the range of unwanted seismic sources such as roads and railroads,
428 industrial buildings with running machines, should be shielded from the signals of wind
429 and rain (at best by burying the sensor several decimetres to metres in the ground) and
430 be installed several kilometres from other neighbouring streams. If the latter is not pos-
431 sible, the Monte Carlo based inversion must include the other stream as an additional
432 source of water turbulence and bedload transport.

433 The approach is vulnerable to transgressive or sudden changes in one or more of
434 the seismic model parameters, for example if soil moisture changes drastically or frozen
435 ground thaws during the summer period, both of which cause changes in the seismic wave
436 velocity and quality factor (James et al., accepted). Likewise, reorganisation of the chan-
437 nel bed by mobilisation, re-deposition, and injection of material, e.g. from bank failures,
438 can change some of the parameters assumed to be stable. Finally, floods beyond bank
439 full depth will result in a sudden and significant change in parameters such as width and
440 depth. Mathematically, the models might be calculated for the different cross sections
441 of the suprabank new river, but this would require setting up more extensive synthetic
442 data sets and exploring the quality of the results of combined model spectra from mul-
443 tiple independent river cross sections.

444 Future applications of the seismic approach introduced here could be near real time
445 warning systems or continuous observation devices for streams otherwise hard to instru-
446 ment, for example due to conservation requirements or steep topography. In principle,

447 it is also possible to survey large, navigable rivers with high bedload fluxes during floods,
 448 as long as the position of the sensor(s) is chosen carefully to minimise the overlap of spec-
 449 tral components and recording of other seismic sources. A continuous record of bedload
 450 transport in combination with high resolution time series of suspended sediment load
 451 opens the perspective for the holistic view on catchment-wide sediment dynamics. Fi-
 452 nally, installation of a series of sensors along a stream over a greater distance allows for
 453 tracking and detailed insight into flood waves, as recently highlighted for a lake outburst
 454 flood in Nepal (Cook et al., 2018). The generic layout of the inversion approach, as il-
 455 lustrated during the seismic parameter range estimation, can in principle be used to in-
 456 vert for parameters other than water depth and bedload transport, as well. Given that
 457 all model parameters are well constrained, one can explore reorganisation of the bed by
 458 comparing model fits with respect to grain-size distribution parameters (s_d and s_s) from
 459 data before and after a flood event.

460 5 Conclusions

461 The seismic method is a valid approach to quantifying key hydraulic and bedload
 462 transport parameters, not merely as proxy data in its own data dimension and unit space
 463 (i.e., dB), but as estimates of the target parameters in the respective units: water depth
 464 in metres and bedload flux in m^3/s or kg/sm . However, this is only possible if i) one or
 465 more stations are placed at appropriate distances from the river as seismic source, ii) the
 466 empirical data are free of (or cleaned from, (e.g., Bottelin et al., 2013)) unwanted sig-
 467 nal components, and iii) the relevant model parameters are sufficiently well constrained,
 468 either by independent measurements or at least by optimising free parameters with re-
 469 spect to the target parameters during a control period. The approach yields a quasi-continuous
 470 output with relative deviations of 0.10 m (water depth) and 0.02 kg/sm (bedload flux),
 471 respectively.

472 The comparably uncomplicated and quick installation, potential of almost real time
 473 data transmission and quick processing render the seismic approach a complementary
 474 source of data otherwise difficult to obtain. This opens up perspectives such as explor-
 475 ing the boundary conditions that control the onset of motion in episodically active river
 476 systems, investigating the coupling of processes that shape different landscape elements
 477 such as rock walls, debris flows, bank failures, and migrating rivers, and deliver high res-
 478 olution field data to long-standing concepts of fluvial geomorphology.

479 The model code has been implemented using a user-driven, free and open software
 480 environment. Sensors and data loggers are becoming more and more affordable. The den-
 481 sity of existing seismic networks along with the availability of their measurement data
 482 increases progressively. These three tendencies provide the base for other scientists to
 483 engage with the method, develop their own measurement systems or make use of the large
 484 amount of existing data to pursue their research hypotheses.

485 Acknowledgments

486 Seismic and stream observatory data, as well as analysis scripts and R functions are avail-
 487 able in the supplementary materials. This study was funded by the Israel Science Foun-
 488 dation grant 832/14 to JBL. MD is funded through the Marie Curie action ITN SUBITOP
 489 (Grant number 674899). All field work was supported by GFZ internal funds.

490 References

- 491 Aberle, J., Coleman, S., & Nikora, V. (2012). Bed load transport by bed form mi-
 492 gration. *Acta Geophysica*, 60, 1720–1743.
- 493 Bagnold, R. (1966). An approach to the sediment transport problem from general
 494 physics. *USGS Special Paper*, 422.

- 495 Barrière, J., Oth, A., Hostache, R., & Krein, A. (2015). Bed load transport monitoring
496 using seismic observations in a low-gradient rural gravel bed stream. *Geo-*
497 *physical Research Letters*, *42*, 2294–2301. doi: 10.1002/2015GL063630
- 498 Bottelin, P., Lèvy, C., Baillet, L., Jongmans, D., & Guèguen, P. (2013). Modal
499 and thermal analysis of les arches unstable rock column (vercors mas-
500 sif, french alps). *Geophysical Journal International*, *194*, 849–858. doi:
501 10.1093/gji/ggt046
- 502 Bunte, K., & Abt, S. (2005). Effect of sampling time on measured gravel bed load
503 transport rates in a coarse-bedded stream. *Water Resources Research*, *41*,
504 W11405. doi: 10.1029/2004WR003880
- 505 Burtin, A., Bollinger, L., Vergne, J., Cattin, R., & Nabelek, J. L. (2008). Spectral
506 analysis of seismic noise induced by rivers: A new tool to monitor spatiotem-
507 poral changes in stream hydrodynamics. *Journal of Geophysical Research*, *113*,
508 B05301. doi: 10.1029/2007JB005034
- 509 Cohen, H., Laronne, J., & Reid, I. (2010). Simplicity and complexity of bed load
510 response during flash floods in a gravel bed ephemeral river: A 10 year field
511 study. *Water Resources Research*, *46*(11). doi: 10.1029/2010WR009160
- 512 Cook, K. L., Andermann, C., Gimbert, F., Adhikari, B. R., & Hovius, N. (2018).
513 Glacial lake outburst floods as drivers of fluvial erosion in the himalaya. *Sci-*
514 *ence*, *362*(6410), 53–57. doi: 10.1126/science.aat4981
- 515 Cudden, J., & Hoey, T. B. (2003). The causes of bedload pulses in a gravel channel:
516 The implications of bedload grainsize distributions. *Earth Surface Processes*
517 *and Landforms*, *28*, 1411–1428.
- 518 Dhont, B., & Ancey, C. (2018). Are bedload transport pulses in gravel bed rivers
519 created by bar migration or sediment waves? *Geophysical Research Letters*,
520 *45*, 5501–5508. doi: 10.1029/2018GL077792
- 521 Dietze, M. (2018). The r package 'eseis' – a software toolbox for environmental seis-
522 mology. *Earth Surface Dynamics*, *6*, 669–686. doi: 10.5194/esurf-6-669-2018
- 523 Dietze, M., Gimbert, F., Turowski, J., Stark, K., Cadol, D., & Laronne, J. (2019).
524 The seismic view on sediment laden ephemeral flows – modelling of ground
525 motion data for fluid and bedload dynamics in the arroyo de los piños [Com-
526 puter software manual]. Retrieved from [https://www.sedhyd.org/2019/](https://www.sedhyd.org/2019/openconf/modules/request.php?module=oc_program&action=view.php&id=99&file=1/99.pdf)
527 [openconf/modules/request.php?module=oc_program&action=view.php&id=](https://www.sedhyd.org/2019/openconf/modules/request.php?module=oc_program&action=view.php&id=99&file=1/99.pdf)
528 [99&file=1/99.pdf](https://www.sedhyd.org/2019/openconf/modules/request.php?module=oc_program&action=view.php&id=99&file=1/99.pdf) (Paper to SEDHYD conference)
- 529 Dietze, M., Turowski, J. M., Cook, K. L., & Hovius, N. (2017). Spatiotemporal pat-
530 terns, triggers and anatomies of seismically detected rockfalls. *Earth Surface*
531 *Dynamics*, *5*(4), 757–779. Retrieved from [https://www.earth-surf-dynam](https://www.earth-surf-dynam.net/5/757/2017/)
532 [.net/5/757/2017/](https://www.earth-surf-dynam.net/5/757/2017/) doi: 10.5194/esurf-5-757-2017
- 533 Einstein, H. (1950). The bedload function for sediment transportation in open chan-
534 nel flows. In *Technical report no. 1026*. United States Department of Agricul-
535 ture.
- 536 Geay, T., Belleudy, P., Habersack, C., Gervaise, H., Aigner, J., Kreisler, A., ...
537 Laronne, J. (2017). Passive acoustic monitoring of bedload flux in a large
538 gravel bed river. *Journal of Geophysical Research*, *128*, 528–545. doi:
539 10.1002/2016JF004112
- 540 Geay, T., Michel, L., Zanker, S., & Rigby, J. R. (2019). Acoustic wave propagation
541 in rivers: an experimental study. *Earth Surface Dynamics*, *7*(2), 537–548. doi:
542 10.5194/esurf-7-537-2019
- 543 Ghilardi, T., Franca, M., & Schleiss, A. J. (2014). Period and amplitude of bedload
544 pulses in a macrorough channel. *Geomorphology*, *221*, 95–103.
- 545 Gimbert, F., B.M., F., M.P., L., Tsai, V., & Johnson, J. (2019). Particle trans-
546 port mechanics and induced seismic noise in steep flume experiments with
547 accelerometer-embedded tracers. *Earth Surface Processes and Landforms*, *44*,
548 219–241. doi: 10.1002/esp.4495
- 549 Gimbert, F., Tsai, V. C., & Lamb, M. P. (2014). A physical model for seismic noise

- 550 generation by turbulent flow in rivers. *Journal of Geophysical Research*, *119*,
551 2209–2238. doi: 10.1002/2014JF003201
- 552 Gomez, B., Naff, R., & Hubbell, D. (1989). Temporal variations in bedload trans-
553 port rates associated with the migration of bedforms. *Earth Surface Processes
554 and Landforms*, *1444*, 135–156.
- 555 Habersack, H., Kreisler, A., Rindler, R., Aigner, J., Seitz, H., Liedermann, M., &
556 Laronne, J. (2016). Integrative automatic and continuous bedload monitoring.
557 *Geomorphology*, *291*, 80–93. doi: 10.1016/j.geomorph.2016.10.020
- 558 Halfi, E., Deshpande, V., Johnson, J., Katoshevski, D., Reid, I., Storz-Peretz, Y., &
559 Laronne, J. (2018). Characterization of bed load discharge in flood bores and
560 very unsteady flows in an ephemeral channel. *E3S Web of Conferences*, *40*,
561 02036. doi: 10.1051/e3sconf/20184002036
- 562 Hildale, R., Carpenter, W., Goodwiller, B., Chambers, J., & Randle, T. (2014).
563 Installation of impact plates to continuously measure bed load: Elwha
564 river, washington, usa. *Journal of Hydraulic Engineering*, *141*. doi:
565 10.1061/(ASCE)HY.1943-7900.0000975
- 566 Iseya, F., & Ikeda, H. (n.d.). Pulsations in bedload transport rates induced by a lon-
567 gitudinal sediment sorting: A flume study using sand and gravel mixtures. *Ge-
568 ografiska Annaler. Series A, Physical Geography*, *69*.
- 569 James, S. R., Knox, H. A., Abbott, R. E., Panning, M. P., & Sreaton, E. J. (ac-
570 cepted). Insights into permafrost and seasonal active-layer dynamics from
571 ambient seismic noise monitoring. *Journal of Geophysical Research: Earth
572 Surface*.
- 573 King, J. G., Emmett, W. W., Whiting, P. J., & Kenworthy, R. P. B. J. J. (2004).
574 Sediment transport data and related information for selected coarse-bed
575 streams and rivers in idaho. general technical report rmrs-gtr-131. In *Gen-
576 eral technical report rmrs-gtr-131* (p. 26). U.S. Department of Agriculture,
577 Forest Service, Rocky Mountain Research Station.
- 578 Laronne, J., Reid, I., Yitshak, Y., & Frostick, L. (1992). Recording bedload dis-
579 charge in a semiarid channel, nahal yatir, israel. *International Association of
580 Hydrological Sciences*, *210*, 79–86.
- 581 Lisle, T., Cui, Y., Parker, G., Pizzuto, J., & Dodd, A. (2001). The dominance of
582 dispersion in the evolution of bed material waves in gravel-bedded rivers. *Earth
583 Surface Processes and Landforms*, *26*, 1409–1420. doi: 10.1002/esp.300
- 584 Mizuyama, T., Laronne, J., Nonaka, M., Sawada, T., Satofuka, Y., Matsuoka, M.,
585 . . . Tsuruta, K. (2010). Calibration of a passive acoustic bedload monitoring
586 system in japanese mountain rivers. *US Geological Survey Scientific Investiga-
587 tions Report*, *5091*, 296–318.
- 588 Parker, G. (1990). Surface-based bedload transport relation for gravel rivers. *Journal
589 of Hydraulic Research*, *28*, 417–436. doi: 10.1080/00221689009499058
- 590 RCoreTeam. (2015). R: A Language and Environment for Statistical Computing
591 [Computer software manual]. Vienna, Austria. Retrieved from [http://CRAN.R-
592 -project.org](http://CRAN.R-project.org)
- 593 Rickenmann, D. (2017). Bedload transport measurements with geophones, hy-
594 drophones and underwater microphones (passive acoustic methods). In
595 D. Tsutsumi & J. Laronne (Eds.), *Gravel bed rivers and disasters* (first edi-
596 tion ed., pp. 185–208). John Wiley & Sons.
- 597 Roth, D. L., Brodsky, E. E., Finnegan, N. J., Rickenmann, D., Turowski, J., &
598 Badoux, A. (2016). Bed load sediment transport inferred from seismic sig-
599 nals near a river. *Journal of Geophysical Research Earth Surface*, *121*. doi:
600 10.1002/2015JF003782
- 601 Roth, D. L., Finnegan, N. J., Brodsky, E. E., Rickenmann, D., Turowski, J. M.,
602 Badoux, A., & Gimbert, F. (2017). Bed load transport and boundary rough-
603 ness changes as competing causes of hysteresis in the relationship between river
604 discharge and seismic amplitude recorded near a steep mountain stream. *Jour-*

- 605 *nal of Geophysical Research Earth Surface*, 122. doi: 10.1002/2016JF004062
606 Schmandt, B., Gaeuman, D., Stewart, R., Hansen, S., Tsai, V., & Smith, J. (2017).
607 Seismic array constraints on reach-scale bedload transport. *Geology*, 45, 299–
608 302. doi: 10.1130/G38639.1
- 609 Schumm, S. (1991). *To interpret the earth: Ten ways to be wrong*. Cambridge Uni-
610 versity Press.
- 611 Schumm, S. (2005). *River variability and complexity*. Cambridge University Press.
- 612 Tsai, V., Minchew, B., Lamb, M. P., & Ampuero, J.-P. (2012). A physical model
613 for seismic noise generation from sediment transport in rivers,. *Geophysical Re-*
614 *search Letters*, 39, L02404. doi: 10.1029/2011GL050255
- 615 Tuszynski, J. (2014). `catools`: Tools: moving window statistics, gif, base64, roc auc,
616 etc. [Computer software manual]. Retrieved from [https://CRAN.R-project](https://CRAN.R-project.org/package=caTools)
617 [.org/package=caTools](https://CRAN.R-project.org/package=caTools) (R package version 1.17.1)
- 618 Welch, P. D. (1967). The use of fast fourier transform for the estimation of power
619 spectra: A method based on time averaging over short, modified periodograms.
620 *IEEE Transactions on Audio and Electroacoustics*, 15, 70–73.